Available online at www.sciencedirect.com
ScienceDirect
Physica B 394 (2007) 86–92
PHYSICA B
www.elsevier.com/locate/physb

The effects of fluorine on the structural, surface morphology and optical properties of ZnO thin films

Fahrettin Yakuphanoglu[a,*], Yasemin Caglar[b], Saliha Ilican[b], Mujdat Caglar[b]

[a]*Firat University, Faculty of Arts and Sciences, Department of Physics, 23169 Elazig, Turkey*
[b]*Anadolu University, Faculty of Science, Department of Physics, 26470 Eskisehir, Turkey*

Received 29 June 2006; received in revised form 12 January 2007; accepted 9 February 2007

Abstract

The optical and structural properties of fluorine-doped Zinc oxide (ZnO) thin films have been investigated. The X-ray diffraction spectra indicate that the films have polycrystalline nature. A ZnO single phase with a hexagonal wurtzite structure was observed in structure of the films. The grain size for the films was calculated using a well-known Scherrer's formula and the obtained values are in the range of 27–40 nm. The values of direct band gap E_g^d were determined and these values change with doped fluorine (F) content. The shift of absorption edge is associated with Burstein–Moss effect. The width of localized states in the optical band of the films change with F content and the E_U values change inversely with optical band gap values of the films.

PACS: 78.20.−e; 78.20.Ci

Keywords: Thin film; Optical band gap; ZnO; Optical constant

1. Introduction

Zinc oxide (ZnO) is a versatile and important semiconductor, which has attracted significant attention because of its characteristic catalytic properties such as transparency in the visible range, direct band gap (3.2–3.4 eV), absence of toxicity, abundance in nature, etc. These properties find wide technological applications. For instance, ZnO-based materials have been used in solar cells, transparent conducting films, chemical sensors, varistors, light-emitting diodes, laser diodes, etc. [1–7].

Physical properties of undoped and doped ZnO films have been widely reported. In spite of extensive studies on preparation, properties and effects of dopants on the properties of ZnO, certain effects of either some dopants or preparation procedures are still remaining unclear. Unlike the effects of indium and other group III elements in ZnO, effect of fluorine is less discussed. ZnO:F is a good candidate to be used as a high-quality transparent electrode in this kind of solar cell.

High-quality ZnO:F films can be deposited by several techniques such as RF-magnetron sputtering [8] and spray pyrolysis [9–13]. The spray pyrolysis method has the advantages of low cost, easy-to-use, safe and can be implemented in a standard laboratory. Despite these advantages, to our knowledge there are few reports of ZnO:F, especially when it is prepared by spray pyrolysis.

To the best knowledge, there are not much publications on the optical characterization of ZnO:F thin films. In this work, the influence of fluorine doping on the structural properties, surface morphology and optical properties of deposited ZnO thin films has been investigated.

2. Experimental

The undoped and F-doped ZnO films were deposited onto glass slices, chemically cleaned, using spray pyrolysis method at 450 °C substrate temperature. 0.2 M solution of zinc acetate dehydrate [$Zn(CH_3COO)_2 \cdot 2H_2O$] diluted in methanol and deionized water (3:1) was used for all the

*Corresponding author.
E-mail addresses: fyhanoglu@firat.edu.tr, fyhan@hotmail.com (F. Yakuphanoglu).

0921-4526/$ - see front matter © 2007 Elsevier B.V. All rights reserved.
doi:10.1016/j.physb.2007.02.014

films, and ammonium fluoride (FNH_4) was added to starting solution for fluorine-doping. Zinc acetate dehydrate and ammonium fluoride solutions were mixed together in different volume proportions ranging from 5% to 15% in steps of 5% (in the volume ratio 1:19, 1:9 and 3:17, to vary the doping concentration of F in ZnO). The F/Zn ratio was 5, 10 and 15% in the solution. A few drops of acetic acid were added to improve the clarity of solution. Nitrogen was used as the carrier gas, pressure at 0.2 bar. The ultrasonic nozzle to substrate distance was 30 cm and during deposition, solution flow rate was held constant at 4 ml/min. The thicknesses of the films were determined with Mettler Toledo MX5 microbalance by using weighing method. The thickness of the films was found to be about 600 nm.

The constants of unit cell were determined from the X-ray diffraction (XRD) patterns, carried out using the RIGAKU RINT 2200 Series X-ray Automatic Diffractometer. Diffractometer reflections were taken at room temperature and values of 2θ were swapped between 20 and 70 with a scanning speed of 2°/min at 40 kV and 30 mA. The incident wavelength is 1.54059 Å. Surface morphology was studied using Atomic Force Microscope (AFM) Solver PRO.

Optical measurements of all the films were carried out at room temperature using Shimadzu UV–VIS-2450 spectrophotometer in the wavelength range from 190 to 900 nm.

3. Results and discussion

3.1. Structural and morphological properties of the thin films

The crystal structure and orientation of the undoped and F-doped ZnO thin films were investigated by XRD measurements. XRD spectra for F-doped ZnO thin films prepared at 450 °C, shown in Fig. 1, indicate that the films are of polycrystalline nature. XRD pattern of the undoped and F-doped ZnO thin films indicate the existence of a ZnO single phase with a hexagonal wurtzite structure.

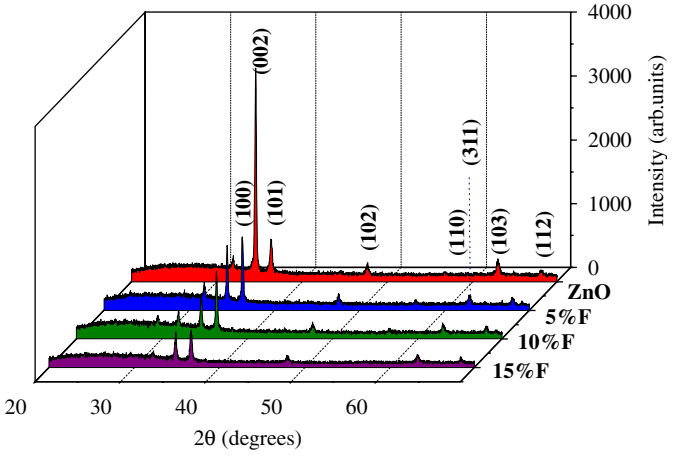

Fig. 1. X-ray diffraction spectra of undoped and F-doped ZnO thin films.

As shown in Fig. 1, undoped film has a preferred orientation with (0 0 2). Another major orientation present is (1 0 1), while other orientations like (1 0 3), (1 0 0) and (1 0 2), are also seen with comparatively lower intensities. Therefore, the crystallites are highly oriented with their *c*-axes perpendicular to the plane of the substrate.

It is seen in Fig. 1 that the crystallinity of ZnO thin films was deteriorated with fluorine incorporation. As shown in Fig. 1, no extra phases involving fluorine compounds were observed, even for the highest [F]/[Zn] contents used. This can be attributed to high volatility of the fluorine at 450 °C. However, the preferential growth is strongly affected by the variation in the fluorine content. Indeed, a dominant signal associated with the (1 0 1) planes is found for F-doped ZnO thin films. The 2θ and d values for the films are given in Table 1.

The lattice constants for hexagonal ZnO film are reported in JCPDS standard data $a = 3.24982$ Å and $c = 5.20661$ Å [14]. The analytical method [15] for calculating lattice constants is used to calculate a and c for the films (Table 2). These calculated values are in agreement with JCPDS data.

The grain size for the films was calculated using a well-known Scherrer's formula. The obtained values are in the range of 27–40 nm. As seen in Fig. 2, the grain size of the films decreases, as the F/Zn ratio increases. This effect can be explained if it is considered that: (a) fluorine atoms do not substitute oxygen atoms, instead they occupy interstitial sites resulting in a large number of dislocations; and (b) probable formation of compound which is growing along with ZnO:F. This behavior of grain size with

Table 1
2θ and d values for the films

(*h k l*)	Undoped ZnO		5% F-doped ZnO		10% F-doped ZnO		15% F-doped ZnO	
	2θ	d (Å)	2θ	d (Å)	2θ	d (Å)	2θ	d (Å)
(1 0 0)	31.899	2.8032	31.741	2.8168	31.941	2.7996	32.241	2.7743
(0 0 2)	34.521	2.5960	34.421	2.6034	34.619	2.5889	34.860	2.5716
(1 0 1)	36.340	2.4702	36.220	2.4781	36.419	2.4650	36.679	2.4481
(1 0 2)	47.658	1.9066	47.500	1.9126	47.699	1.9051	47.919	1.8968
(1 1 0)	–	–	56.498	1.6275	56.660	1.6232	–	–
(1 0 3)	62.940	1.4755	–	–	62.940	1.4755	63.219	1.4697
(3 1 1)	–	–	62.800	1.4785	–	–	–	–
(1 1 2)	–	–	67.840	1.3804	68.040	1.3768	68.242	1.3732

Table 2
Calculated a and c lattice constants for the films

	Undoped ZnO	5% F-doped ZnO	10% F-doped ZnO	15% F-doped ZnO
a (Å)	3.23686	3.25256	3.23270	3.23690
c (Å)	5.19200	5.20680	5.17780	5.19200

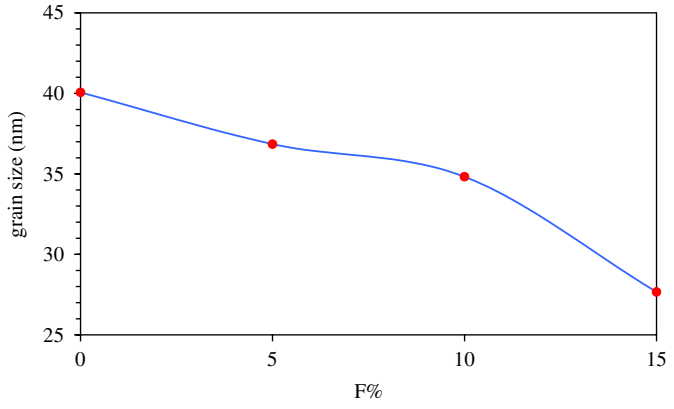

Fig. 2. Variation of grain size with fluorine content in ZnO films.

increasing the doping level is in agreement with those reported for ZnO thin films prepared by the same process [11,12].

The texture coefficient (TC) represents the texture of a particular plane, deviation of which from unity implies the preferred growth. Quantitative information concerning the preferential crystallite orientation was obtained from different texture coefficient TC($h\,k\,l$) defined by well-known relation,

$$\mathrm{TC}(h\,k\,l) = \frac{I(h\,k\,l)/I_o(h\,k\,l)}{N^{-1}\sum_n I(h\,k\,l)/I_o(h\,k\,l)}, \quad (1)$$

where $I(h\,k\,l)$ is the measured relative intensity of a plane ($h\,k\,l$), $I_o(h\,k\,l)$ is the standard intensity of the plane ($h\,k\,l$) taken from the JCPDS data, N is the reflection number and n is the number of diffraction peaks. A sample with randomly oriented crystallite presents TC($h\,k\,l$) = 1, while the larger this value, the larger abundance of crystallites oriented at the ($h\,k\,l$) direction. The texture coefficients calculated for the two main diffraction peaks, i.e., (0 0 2) and (1 0 1), are given in Table 3.

The variation of texture coefficient for (0 0 2) and (1 0 1) planes with the fluorine content is shown in Fig. 3. It can be seen that the highest TC was in (0 0 2) plane for undoped ZnO thin film and in (1 0 1) plane for the doped ZnO thin films.

The two-dimensional images obtained from AFM for the undoped and 15% doped ZnO thin films are shown in Fig. 4. Also root mean square (RMS) values of surface roughness are given in these figures. The films demonstrate a porous structure. ZnO particles can be clearly observed in both the low (Fig. 4a and c) and high magnification images (Fig. 4b and d). The deposits appear to be composed of randomly distributed islands in low-magnification image. From the high-magnification image, square, cluster-shaped deposits are clearly observed. For the characterization of these films, it is important to determine their RMS roughness. It can be seen that the crystallinity of the films deteriorates and the crystallite size become smaller with fluorine contents which is shown by XRD analysis; also the degree of surface roughness increases.

Table 3
Relative intensity of the peaks (I/I_o) and TC($h\,k\,l$) values of the films

	Undoped ZnO		5% F-doped ZnO		10% F-doped ZnO		15% F-doped ZnO	
($h\,k\,l$)	I/I_o	TC($h\,k\,l$)	I/I_o	TC($h\,k\,l$)	I/I_o	TC($h\,k\,l$)	I/I_o	TC($h\,k\,l$)
(1 0 0)	4.9	0.1846	20.1	0.5706	22.5	0.7038	17.4	0.3859
(0 0 2)	100	3.7679	80.8	2.2936	53.5	1.6734	91.1	2.0199
(1 0 1)	15.4	0.5803	100	2.8386	100	3.1278	100	2.2173
(1 0 2)	4.9	0.1846	15.6	0.4713	15.3	0.4786	22.5	0.4989
(1 0 3)	7.5	0.2826	–	–	15.5	0.4848	22.2	0.4989
(1 1 0)	–	–	5.5	0.1561	7.1	0.2221	–	–
(1 1 2)	–	–	11.2	0.3179	9.9	0.3097	17.1	0.3792
(3 1 1)	–	–	12.4	0.3520	–	–	–	–

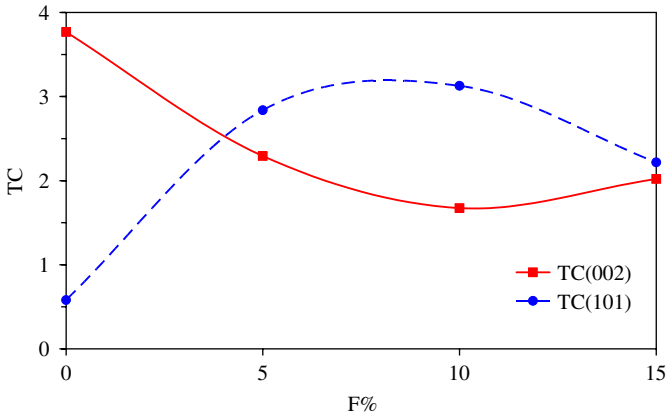

Fig. 3. Variation of TC(0 0 2) and TC(1 0 1) with fluorine content in ZnO films.

3.2. Optical properties of the thin films

Transmittance and reflectance of the films are shown in Figs. 5(a, b). The films exhibit a fundamental fall in transmittance at about 375 nm. For wavelength less than 375 nm, a peak was observed at 3.4 eV and was attributed to the exciton transition. The exciton effect is closely linked with film quality. The exciton effect has been observed in ZnO at room temperature [16]. The absorption edge shifts from lower wavelength region to higher wavelength with the increase of F content. The optical band gap can be calculated from the following relationship [17],

$$(\alpha h\nu) = A(h\nu - E_g)^m, \quad (2)$$

where m is a constant which determines type of the optical transition ($m = 1/2$ for allowed direct transitions and $m = 2$ for allowed indirect transitions). Here, the direct and indirect transitions are optical transitions that occur in the crystalline semiconductors. It is well known that direct transition across the band gap is feasible between the valence and the conduction band edges in k space. In the transition process, the total energy and momentum of the electron–photon system must be conserved. Figs. 6(a,b) show plots of $(\alpha h\nu)^2$ vs. photon energy. The values of direct

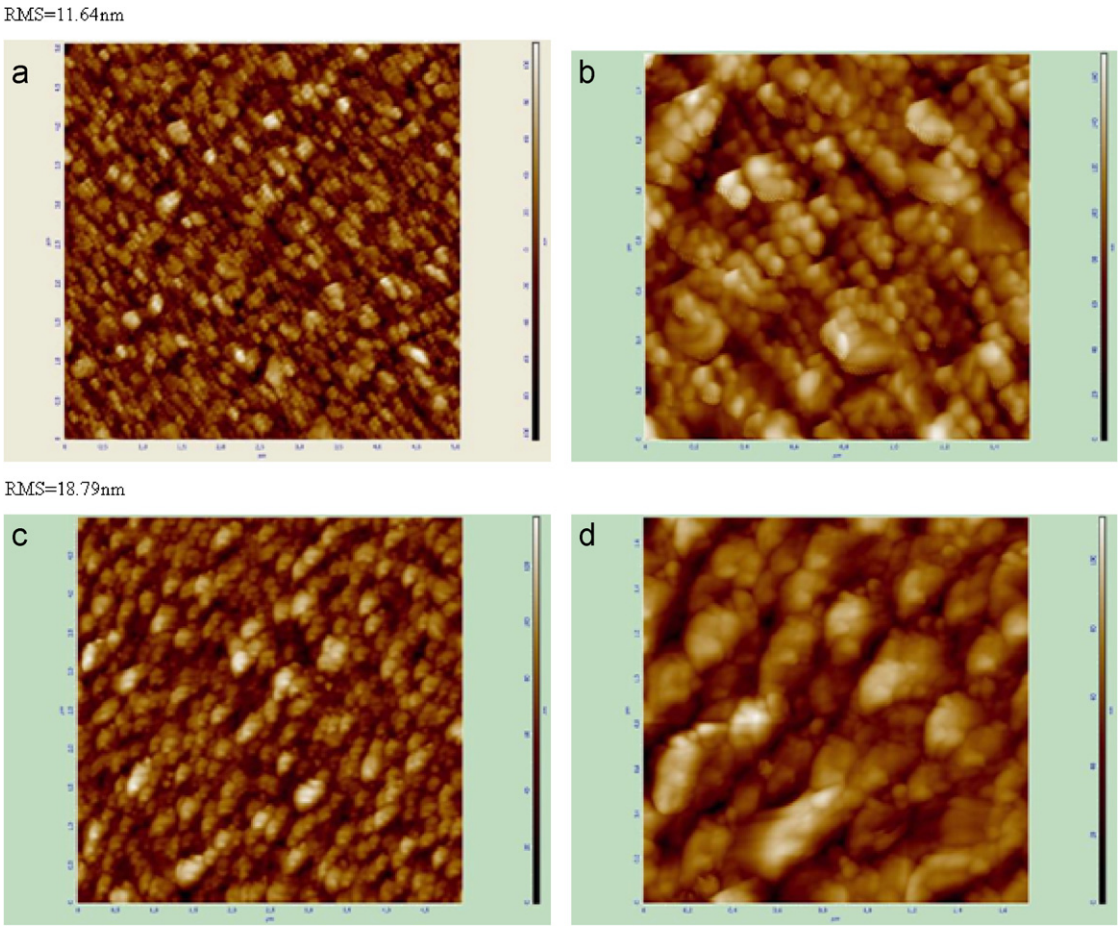

Fig. 4. Two-dimensional AFM images for the ZnO thin films for undoped and 15% fluorine-doped, respectively (a, b—undoped; c, d—15% doped).

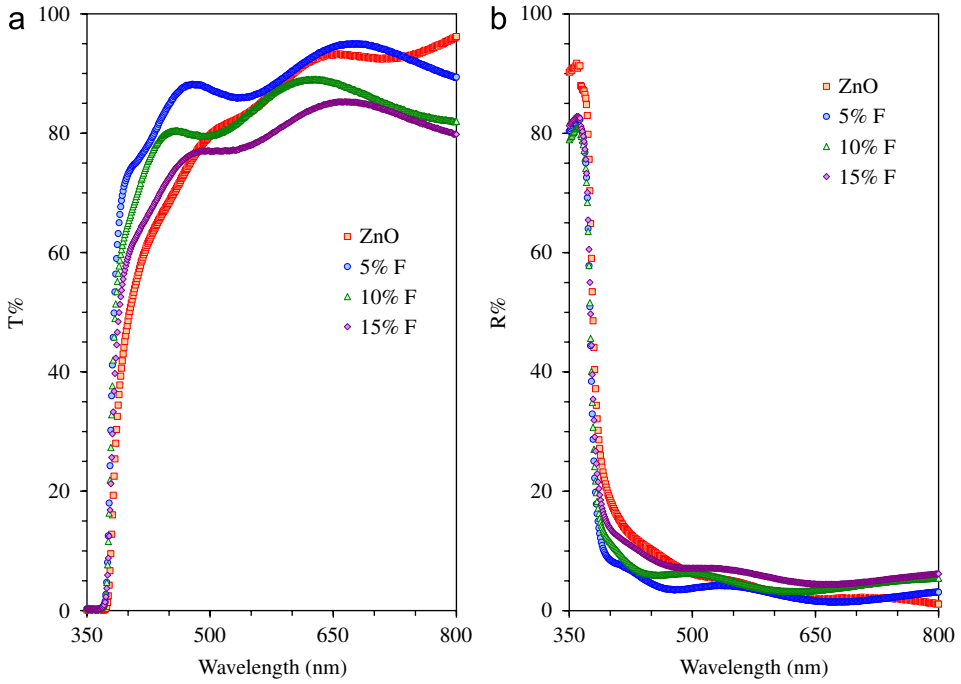

Fig. 5. Optical transmittance (a) and reflectance (b) spectra of undoped and F-doped ZnO thin films.

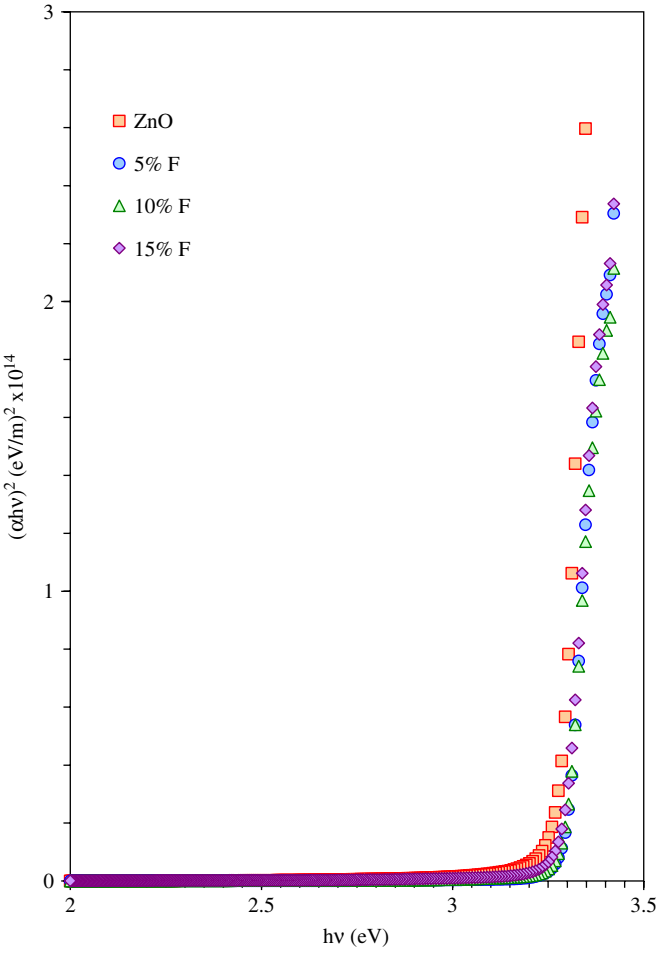

Fig. 6. Plots of $(\alpha h\nu)^2$ vs. photon energy of undoped and F-doped ZnO thin films.

Table 4
The optical parameters of the films

Films	E_g^d (eV)	E_U (meV)	β
ZnO	3.285	575.7	4.48×10^{-2}
5% F	3.295	498.3	5.17×10^{-2}
10% F	3.296	438.7	5.88×10^{-2}
15% F	3.295	729.9	3.53×10^{-2}

band gap E_g^d were determined and are given in Table 4. E_g^d values change with F-doped concentration. The shift of absorption edge is associated with Burstein–Moss effect. The lifting of the Fermi level into the conduction band of degenerate semiconductor leads to the energy band broadening (blue shift) effect. This effect explains the fact of increase of carrier concentration blocking lowest states in the conduction band [18].

The absorption coefficient near fundamental absorption edge is exponentially dependent on the incident photon energy and obeys the empirical Urbach relation, where $\ln \alpha$ varies as a function of $h\nu$. Urbach energy can be calculated by the following relation [19],

$$\alpha = \alpha_o \exp\left[\frac{h\nu - E_I}{E_U}\right], \tag{3}$$

where E_I and α_o are constants and E_U is the Urbach energy which refers the width of the exponential absorption edge. Fig. 7 shows the variation of $\ln \alpha$ vs. photon energy for the films. The E_U value was calculated from Urbach plots using relationship,

$$E_U = \left(\frac{d(\ln \alpha)}{d(h\nu)}\right)^{-1} \tag{4}$$

and calculated values are given in Table 4. Urbach energy values of the films (except for 15% F content) decrease with increasing F content. The F content is responsible for the width of localized states in the optical band of the films and it decreases the width of localized states in the optical band gap. The E_U values change inversely with optical band gaps of the films. In both crystalline and amorphous materials are no known origin of the exponential dependence of absorption coefficient on energy. This dependence may arise from the random fluctuations of internal fields associated with the structural disorder in many amorphous

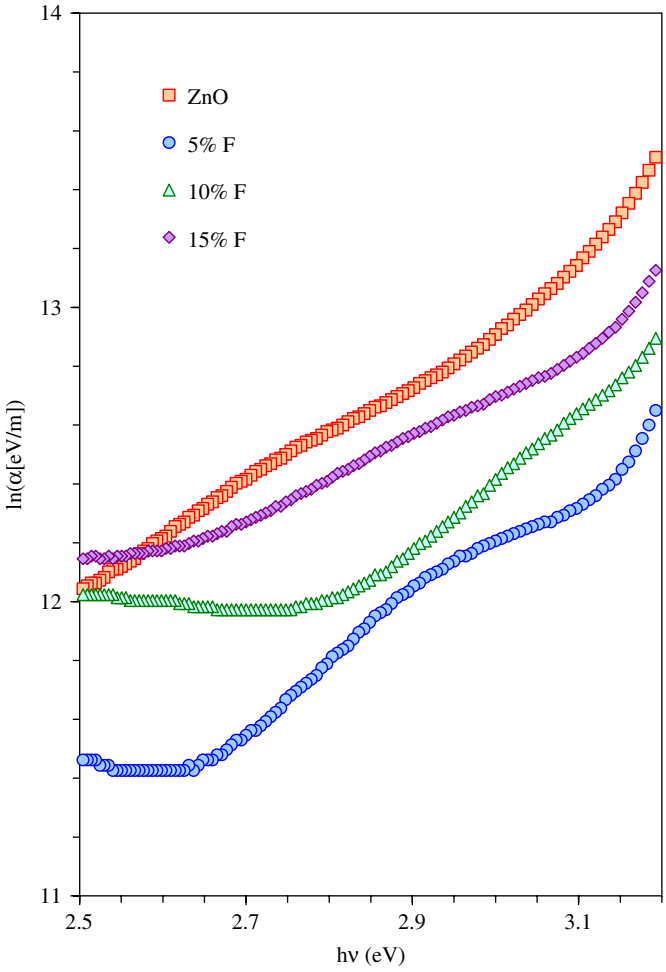

Fig. 7. Urbach plots of undoped and F-doped ZnO thin films.

materials [17]. The dependence of optical absorption coefficient with photon energy may arise from electronic transitions between localized states. The density of these states falls off exponentially with energy which is consistent theory of Tauc [17]. Eq. (6) can be rewritten as

$$\alpha = \alpha_o \exp\left[\frac{\beta}{kT}(E - E_I)\right], \quad (5)$$

where β is called steepness parameter, which characterizes the broadening of the absorption edge due to the electron–phonon interaction or excition–phonon interaction. The β values were calculated using Eq. (5) and taking $T = 300$ K and are given in Table 4. The β values suggest that the absorption edge changes with F content.

3.3. The refractive index and dielectric constants of the films

The complex refractive index and dielectric function characterize the optical properties of any solid material and dispersion plays an important role in the research for optical materials. Because, it is a significant factor in optical communication and in designing devices for spectral dispersion. The complex refractive index of the films is expressed as [20],

$$\hat{n} = n(\omega) + ik(\omega), \quad (6)$$

where n is the real part and k is the imaginary part of complex refractive index. The refractive index of the films can be determined by the following relations

$$T = \frac{(1-R)^2 e^{-\alpha d}}{1 - R^2 e^{-2\alpha d}}, \quad (7)$$

where T is the transmittance, α is the absorption coefficient, d is the thickness of thin film and R is the reflectance, which is expressed as [20],

$$R = \frac{(n-1)^2 + k^2}{(n+1)^2 + k^2}, \quad (8)$$

where n is the refractive index and k ($k = \alpha\lambda/4\pi$) is extinction coefficient. The refractive index values of the films were calculated using Eqs. (7)–(8). The refractive index dependence of wavelength was plotted, as shown in Fig. 8a. As seen in plotted figure of refractive index, the refractive index decreases with wavelength. The change in the refractive index is a result of the F content. The extinction coefficient k's dependence on wavelength is shown in Fig. 8b. The k values of the films decrease up to certain value of wavelength and then increase. The F content changes the k values of the films. The decrease and increase in the n and k values in visible region can be attributed to the decrease and increase of optical absorption in visible region when increasing F content. The fundamental electron excitation spectrum of the films was described by means of a frequency dependent of the complex electronic dielectric constant. The dielectric constant is defined as, $\varepsilon(\omega) = \varepsilon_1(\omega) + i\varepsilon_2(\omega)$ and real and imaginary parts of the dielectric constant are related to the

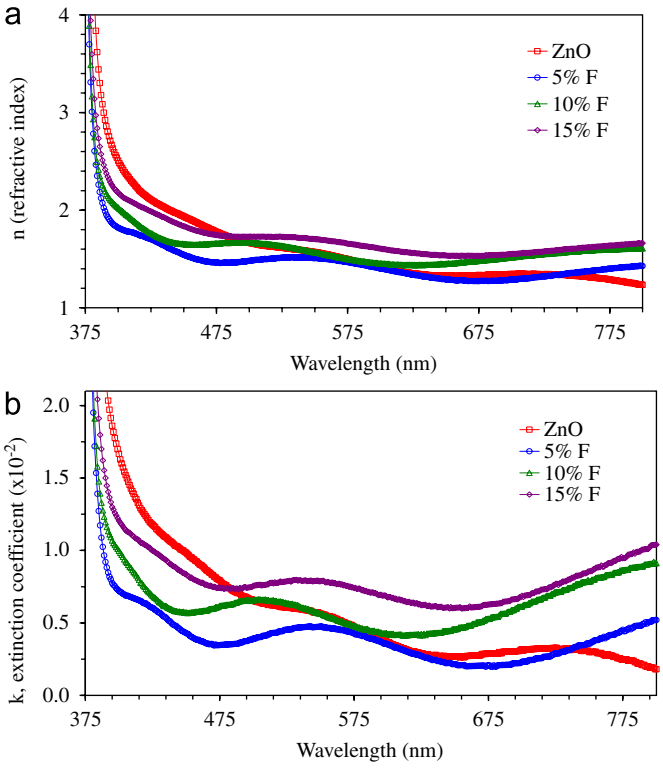

Fig. 8. The variation of refractive index (a) and extinction coefficient (b) of undoped and F-doped ZnO thin films.

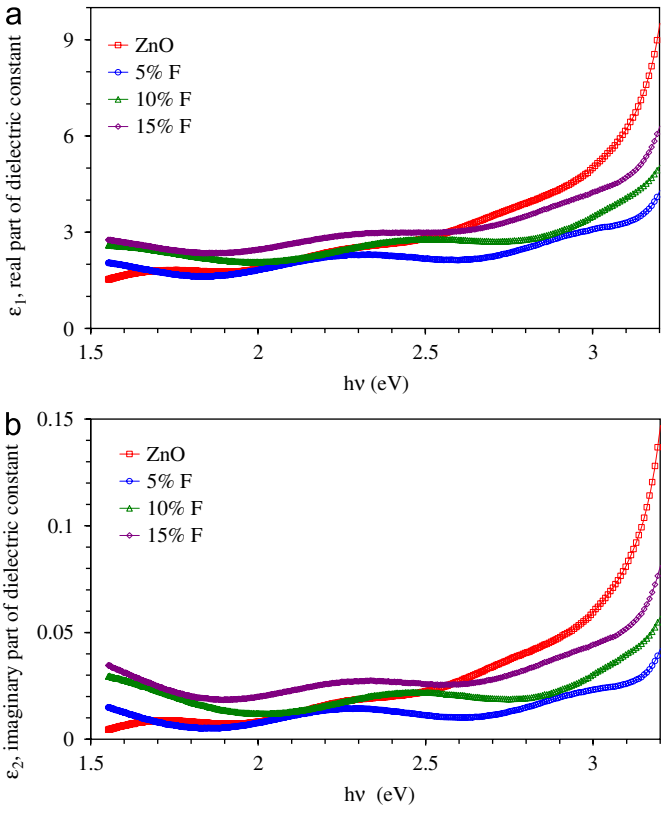

Fig. 9. Variation of real (a) and imaginary (b) parts of the dielectric constant of undoped and F-doped ZnO thin films.

n and k values. The ε_1 and ε_2 values were calculated using the formulas [20],

$$\varepsilon_1 = n^2 - k^2 \quad (9)$$

$$\varepsilon_2 = 2nk. \quad (10)$$

Figs. 9(a,b) show ε_1 and ε_2 values' dependence of photon energy. ε_1 and ε_2 values of the films increase with increasing energy.

4. Conclusions

The optical, surface morphology and structural properties of F-doped ZnO thin films have been investigated. The XRD spectra indicate that the films are of polycrystalline nature. The grain size of crystallites was found to be in the range of 27–40 nm. The values of direct band gap E_g^d change with F-doped concentration. The shift of absorption edge is associated with Burstein–Moss effect. The width of localized states in the optical band gap of the films change with F concentration and the E_U values change inversely with optical band gaps of the films.

Acknowledgments

We are grateful to Anadolu University Department of Materials Science and Engineering for the XRD measurements and Ankara University Department of Engineering Physics for the AFM measurements.

References

[1] V. Sittinger, F. Ruske, W. Werner, B. Szyszka, B. Rech, J. Hüpkes, G. Schöpe, H. Stiebig, Thin Solid Films 496 (2006) 16.
[2] W.J. Jeong, S.K. Kim, G.C. Park, Thin Solid Films 506 (2006) 180.
[3] M. Mikawa, T. Moriga, Y. Sakakibara, Y. Misaki, K. Murai, I. Nakabayashi, K. Tominaga, Mater. Res. Bull. 40 (2005) 1052.
[4] S. Lee, E. Shim, H. Kang, S. Pang, J. Kang, Thin Solid Films 473 (2005) 31.
[5] M.-H. Wang, K.-A. Hu, B.-Y. Zhao, N.-F. Zhang, Mater. Chem. Phys. 100 (2006) 142.
[6] H. Kim, J.S. Horwitz, W.H. Kim, A.J. Mäkinen, Z.H. Kafafi, D.B. Chrisey, Thin Solid Films 420 (2002) 539.
[7] H. Nanto, T. Morita, H. Habara, K. Kondo, Y. Douguchi, T. Minami, Sens. Actuators B: Chem. 36 (1996) 384.
[8] B.G. Choi, I.H. Kim, D.H. Kim, K.S. Lee, T.S. Lee, B. Cheong, Y.-J. Baik, W.M. Kim, J. Eur. Ceram. Soc. 25 (2005) 2161.
[9] M. de la L. Olvera, A. Maldonado, R. Asomoza, O. Solorza, D.R. Acosta, Thin Solid Films 394 (2001) 242.
[10] A. Maldonado, S. Tirado-Guerra, M. Melendez-Lira, M. de la L. Olvera, Sol. Energy Mater. Sol. Cells 90 (2005) 742.
[11] P.M. Ratheesh Kumar, C. Sudha Kartha, K.P. Vijayakumar, F. Singh, D.K. Avasthi, Mater. Sci. Eng. B 117 (2005) 307.
[12] A. Sanchez-Juarez, A. Tiburcio-Silver, A. Ortiz, Sol. Energy Mater. Sol. Cells 52 (1998) 301.
[13] M. de la L. Olvera, A. Maldonado, R. Asomoza, M. Melendez-Lira, Sol. Energy Mater. Sol. Cells 71 (2002) 61.
[14] Joint Committee on Powder Diffraction Standards, Powder Diffraction File, card no.: 36-1451.
[15] B.D. Cullity, S.R. Stock, Elements of X-ray Diffraction, third ed., Prentice Hall, Englewood Cliffs, NJ, 2001.
[16] Z.K. Tang, G.K.L. Wong, P. Yu, M. Kawasaki, A. Ohtomo, H. Koinuma, Y. Segawa, Appl. Phys. Lett. 72 (1998) 3270.
[17] J. Tauc, Amorphous and Liquid Semiconductors, Plenum Press, New York, 1974.
[18] E. Burstein, Phys. Rev. 93 (1954) 632.
[19] F. Urbach, Phys. Rev. 92 (1953) 1324.
[20] A.K. Wolaton, T.S. Moss, Proc. R. Soc. A 81 (1963) 5091.